Applied Catalysis B: Environmental 105 (2011) 50–60

Contents lists available at ScienceDirect

Applied Catalysis B: Environmental

journal homepage: www.elsevier.com/locate/apcatb

Cobalt–polypyrrole–carbon black (Co–PPY–CB) electrocatalysts for the oxygen reduction reaction (ORR) in fuel cells: Composition and kinetic activity

Danh Nguyen-Thanh [a], Anatoly I. Frenkel [b], Jianqiang Wang [b,c], Stephen O'Brien [a], Daniel L. Akins [a,*]

[a] Center for the Exploitation of Nanostructures in Sensor and Energy Systems (CENSES), The City College of New York, 160 Convent Avenue, New York, NY 10031, USA
[b] Physics Department, Yeshiva University, 245 Lexington Avenue, New York, NY 10016, USA
[c] China Petroleum & Chemical Corporation, Shanghai Research Institute of Petrochemical Technology, 1658 Pudong Beilu, Pudong, Shanghai 201208, China

ARTICLE INFO

Article history:
Received 14 November 2010
Received in revised form 17 March 2011
Accepted 28 March 2011
Available online 5 April 2011

Keywords:
Oxygen reduction reaction
EXAFS
Nonprecious metal electrocatalysts
Polypyrrole
PEMFCs

ABSTRACT

Electrocatalysts consisting of polypyrrole (PPY) and Co deposited on carbon black (CB) at several compositions were prepared and tested for the oxygen reduction reaction (ORR) in a $HClO_4$ buffer (pH = 1) using a rotating ring-disk electrode (RRDE). It was determined that the most favorable catalyst composition (prior to calcination) had a CB:PPY weight ratio of 2 and a pyrrole:Co (i.e., PY:Co) molar ratio of 4. This catalyst had an onset potential of 0.785 V (vs. RHE) and a mass activity of *ca.* 1 A/g_{cata} at the fuel cell relevant voltage of 0.65 V. Furthermore, it was found that the number of electrons exchanged during the ORR with the catalyst was *ca.* 3.5 and resulted in 28% yield of H_2O_2 at 0.65 V, which hints to an indirect $4e^-$ reduction of O_2 to H_2O, with H_2O_2 as an intermediate. From energy dispersive spectroscopy (EDS) and extended X-ray absorption fine structure (EXAFS) analysis, it is proposed that a PY:Co ratio of 4 favors the formation, prior to calcination, in the catalyst precursor of Co–N complexes in which Co is coordinated to 3 or 4 N atoms, resulting in strong Co–N interactions that limit the formation upon calcination of low ORR activity Co nanoparticles. These Co–N complexes give rise upon calcination to CoN_{x-2} sites in which the coordination of Co could favor the adsorption on them of O_2, which would make those sites particularly active and selective. At the same mass activity of 1 A/g_{cata}, the voltage yielded by the catalyst was 200 mV lower than that for a state-of-the-art Pt (10 wt.%) catalyst, whose H_2O_2 output at 0.85 V was 39% and involves the exchange of $3.2e^-$, overall making our material an attractive substitute to noble metal ORR electrocatalysts.

1. Introduction

Fuel cells are increasingly perceived as clean, efficient, and dependable sources of energy, and are anticipated to become ubiquitous in the near future. Indeed, their applications include portable electronics, transportation, and industrial and residential power sources. However, major obstacles remain to the widespread use of fuel cell technology. The hurdles derive from identifying appropriate fuels, frequently hydrogen (production and distribution), and creating commercially viable fuel cells.

Although current fuel cells offer adequate performances, their costs remain too high for wide-spread use, particularly in the case of the proton exchange membrane fuel cell (PEMFC), the expected successor to the internal combustion engine in vehicles. The cost of PEMFCs is mainly due to the use at the electrodes of electrocatalysts with high loadings of Pt (typically 10–60 wt.%) that enhance the otherwise slow kinetics of electron transfer. The redox reactions involved in the PEMFC are depicted below:

$$\text{Anode (oxidation)} \quad H_2 \rightarrow 2H^+ + 2e^- \qquad E^o_{anode} = 0.00\,V$$

$$\text{Cathode (reduction)} \quad O_2 + 4H^+ + 4e^- \rightarrow 2H_2O \qquad E^o_{cathode} = 1.23\,V$$

It is estimated that Pt alone can represent up to 71% of the cost of a PEMFC [1]. And since most of that Pt is located at the cathode, considerably less expensive PEMFCs could be obtained by replacing Pt there with nonprecious metal alternatives for the oxygen reduction reaction (ORR) in acidic medium.

A class of nonprecious metal ORR electrocatalysts that has received considerable attention is one that consists of Co or Fe coordinated to a macrocycle such as porphyrin or phthalocyanine. The activities of such catalysts were first reported more than 40 years ago for Co-phthalocyanine compounds [2]. It was later shown that pyrolysis of these macrocycle complexes at temperatures between 600 and 1000 °C under an inert atmosphere improved their activities and stabilities [3,4]. The ORR activities of such catalysts are widely believed to originate from the presence of MeN_x sites (where Me is typically Fe or Co). Since the existence of Me–N bonds appears

* Corresponding author. Tel.: +1 212 650 6953; fax: +1 212 650 6848.
E-mail address: akins@sci.ccny.cuny.edu (D.L. Akins).

0926-3373/$ – see front matter © 2011 Elsevier B.V. All rights reserved.
doi:10.1016/j.apcatb.2011.03.034

decisive for the ORR, other sources of N, sometimes less expensive and easier to handle, have recently been used to form MeN_x sites on a C surface. Such N sources include, for example, NH_3 [5,6], tripyridyltriazine [7], triethylenetetramine [8], ethylene diamine [9], and polypyrrole (PPY) [10–13]. The latter compound, PPY, is an especially interesting N precursor since it is a conducting polymer. Moreover, the aromaticity of the pyrrole (PY) ring should imbue the polymer with some strong affinity for graphitic carbon, the typical support in ORR electrocatalysts. However, the composition of catalysts consisting of PPY and Co has apparently not been optimized, since compositions usually differ between publications, with C to PPY weight ratios ranging between 5:1 and 1:5, and PY to Co molar ratios between 1.3 and 6.6; also, the overall Co content varies between 3.5 and 31 wt.%. Furthermore, published studies indicate the use of different carbon supports, like carbon black [10,11,13] or multiwalled carbon nanotubes (MWNTs) [12], all with differing degrees of graphitization and surface areas.

The lack of optimization for the aforementioned PPY/Co catalysts may be due partially to the fact that the exact nature of the catalytic sites remains unclear and is still the subject of controversy. Indeed, as has been mentioned previously, it is generally understood and accepted that MeN_x sites are responsible for ORR in such materials, with the coordination of Me determining the degree of catalytic activity [6,14]. However, some researchers suggest that the N atoms are the actual active sites, with Me only catalyzing the incorporation of N into the C matrix [9,15].

The main objectives of the present article are to study the influence of composition of PPY/Co catalysts on the ORR activity using Vulcan XC-72 as the carbon black (CB) support and to identify the active sites in such catalysts. Inherent in our efforts is to compare the performance of catalysts that we prepare with that of a commercial Pt-based catalyst and to ascertain whether PPY/Co catalysts represent a viable alternative to precious metal ones in fuel cells. For comparison, we have chosen the state-of-the-art Pt-based (10 wt.%) catalyst ETEK from BASF, whose support is also Vulcan XC-72.

2. Experimental

CB coated with PPY was prepared following a simple procedure. Specifically, for a CB:PPY weight ratio of 2:1, 300 mg of CB and 150 μL of PY (144.9 mg) were dispersed in 50 mL of water. The suspension was maintained under vigorous agitation for 2 h. Then an amount of $FeCl_3{\cdot}6H_2O$ corresponding to a Fe:PY molar ratio of 2.5:1 dissolved in water was added dropwise to the suspension and stirred for another 24 h. The suspension was then filtered and the filtrate was washed sequentially with 4 L of warm water, 50 mL of acetone, and 50 mL of ethanol. The complete removal of chloride anions was confirmed by testing the last 50 mL of filtrate with 1 M $AgNO_3$. Based on the absence of formation of AgCl, it is assumed that most of the ferric cations was also removed from the retentate. The resultant support was then dried under vacuum at a temperature between 60 and 100 °C for 6 h. Weighing of the materials after drying showed that essentially 100% of the PY had polymerized.

Impregnation of the PPY/CB supports was accomplished in the same fashion for all the samples. Typically, 200 mg of the PPY/CB support and a quantity of $Co(CH_3COO)_2{\cdot}4H_2O$ that agreed with the desired PY:Co molar ratio was dispersed in 35 mL of water and the suspension was stirred for 2 h at 80 °C under reflux. A quantity of $NaBH_4$ that corresponded to a $NaBH_4$:Co molar ratio of 10:1 dissolved in 15 mL of water was then added to the suspension, and the resulting suspension was refluxed at 80 °C for 4 h under an inert N_2 atmosphere. After filtering the suspension, the catalyst was washed, sequentially, with 1.5 L of warm water, 50 mL of acetone, and 50 mL of ethanol, then subsequently dried for 6 h in the 60–100 °C range under vacuum. Determination of the samples' masses indicated that all the Co used was indeed loaded into the supports.

The catalysts were then placed in quartz boats and calcined in a tube (1 in. diameter) furnace at 400 °C (2 h) and 900 °C (2 h) under Ar (100 mL/min) with a temperature ramp of 10 °C/min. Having conducted preliminary survey tests over the 600–900 °C region, we had found that 900 °C was the optimum calcination temperature for ORR activity. The catalysts in this paper are referred to as Co_pPPYCB_m, in which m represents the CB:PPY weight ratio and p the PY:Co molar ratio.

Powder X-ray diffraction (XRD) experiments were carried out with a Philips X'Pert X-ray diffractometer using Cu K_α radiation (1.54056 Å) at a scan rate of 0.02°/s; scans were conducted at 45 kV and 40 mA.

Transmission electron microscopy (TEM) was accomplished with a Zeiss EM 902 (80 kV). The samples were dispersed by sonication in ethanol, then deposited on a carbon-coated copper grid and left to dry in air. Distances in the micrographs were determined through using the ImageJ software.

Scanning electron microscopy (SEM) was performed using a Zeiss Supra 55 VP. The instrument also has energy dispersive X-ray spectroscopy (EDS) capability, which was used to determine the N:Co atomic ratios of the catalysts. For each EDS experiment, the voltage was set at 15 kV and a dozen particles that were at least around 2 μm wide were analyzed.

X-ray absorption experiments were completed at beamline X19A of the National Synchrotron Light Source at Brookhaven National Laboratory. The beamline uses a Si (1 1 1) double-crystal monochromator. X-ray absorption data were collected at room temperature in the transmission mode. Gas ion chamber detectors were used for incident, transmitted, fluorescence, and reference channels. The specimens were prepared by brushing the powders over an adhesive tape and folding it several times for uniformity. Some samples were also made as pellets by applying 5-ton pressure using a hydraulic press. Reference Co spectra were obtained simultaneously in the transmission mode for all sample scans using Co foil. Data processing and analysis were done with IFEFFIT software [16].

Electrochemical experiments were performed using a rotating ring-disk electrode (RRDE). The working electrode consisted of a glassy carbon disk (5 mm diameter) and a Pt ring (6.5 mm ID and 7.5 mm OD). The counter electrode was a Pt wire. The reference electrode was a double junction Ag/AgCl electrode (0.210 V vs. RHE). Potentials at the working electrode were controlled through a AFCBP1 bipotentiostat from Pine Research Instrumentation, which also measured currents. The entire setup was controlled by a PC through use of the AfterMath Module ASCBA01 software. Throughout this paper, all potentials are quoted referenced to the RHE. A buffer of 0.1 M $HClO_4$ was used. The thermodynamic potential for ORR in our experiments (at pH 1) was 1.17 V.

To deposit the catalysts on the disk, inks were prepared by dispersing the catalysts using a sonicating bath for 10 min, in an aqueous solvent containing 40 vol.% of ethanol (EW40) in a 15 mm × 45 mm vial. To estimate the amount of catalyst on the disk, a volume of ink was sampled from the vial, using a gastight syringe with a blunt needle, by drawing equal amounts at four equidistant points at the bottom circumference of the vial. Then each particular ink sample was deposited in a weighing dish and left to dry under air. Midway through sampling (after drawing two samples), 10 μL of ink was removed from the vial and placed on the disk. The ink was left to dry under air, then 8 μL of a solution of 5 wt.% Nafion (15–20% water) diluted to 1 wt.% with EW40 was dropped onto the disk to affix the catalyst. The composition of the inks and the amounts sampled are reported in Table 1.

Table 1
Catalyst inks compositions and amounts of catalyst deposited on the carbon disk.

	m_{cata} (mg)	V_{EW40} (μL)	$V_{sampled}$ (μL)	$m_{sampled}$ (mg)	m_{cata} (μg)
ETEK	5	250	150	1.0	70
$Co_2PPYCB_{0.5}$	30	100	110	1.1	100
Co_2PPYCB_1	20	100	110	1.1	100
Co_2PPYCB_2	15	250	150	1.2	80
Co_2PPYCB_4	5	250	150	1.0	70
Co_4PPYCB_2	20	250	150	1.6	110
Co_1PPYCB_2	15	250	150	1.8	120

Prior to any ORR experiment, ultrapure N_2 was bubbled through the buffer for 30 min, followed by blanketing the buffer solution with a stream of N_2 gas. The electrode (without rotation) was cycled a dozen times between 0.01 and 1.21 V at 50 mV/s for electrochemical conditioning, after which reproducible scans were obtained. For ORR experiments, which consisted of cyclic voltammetry (CV) and linear sweep voltammetry (LSV), the buffer solution was degassed with ultrapure O_2 for 20 min before blanketing with O_2. Following the ORR experiments, a second N_2 treatment (bubbling and blanketing) was applied to the buffer, but this time to record the capacitive currents, carrying out CV and LSV experiments under the same conditions (sweep and rotation rates) as the ones used with O_2. CV and LSV experiments were conducted at a sweep rate of 10 mV/s, with rotational rates between 500 and 2000 rpm when using the rotating disk electrode (RDE) setup only (i.e., without applying any potential to the ring in the RRDE). RRDE experiments were conducted at a rotation rate of 1500 rpm, a ring potential of 1.31 V (at which the oxidation of peroxide is diffusion-limited), and a sweep rate of 5 mV/s. The collection efficiency (N) of the RRDE was found to be 0.22, as determined by the reduction at the disk of $[Fe(CN)_6]^{3-}$ at 1500 rpm, the theoretical value of N being 0.256, as stated by the manufacturer. The disk currents from ORR obtained by LSV were corrected by subtracting the capacitive currents.

3. Results

The first step in our ORR activity study was to determine the CB:PPY weight ratio (m) that yielded the best catalytic activity for ORR. To that end, four catalysts with identical PY:Co molar ratios of $p = 2$, but with CB:PPY weight ratios of $m = 0.5$, 1, 2, and 4 were prepared and tested for ORR by CV and LSV. CV results are plotted in Fig. 1 and reported in Table 2. The criterion for ORR activity was the position of the negative cathodic peak, $E_{P,C}$, that corresponds

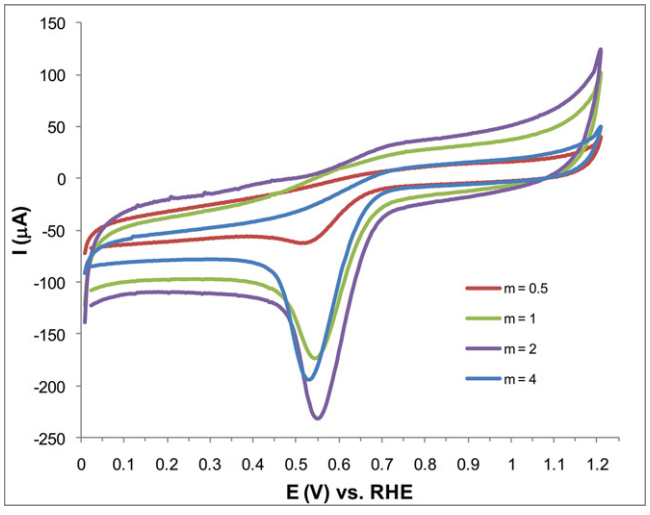

Fig. 1. Cyclic voltammetry of catalysts with different CB:PPY weight ratios m and equal PY:Co molar ratios $p = 2$ at a scan rate of 10 mV/s, in a $HClO_4$ buffer at pH = 1.

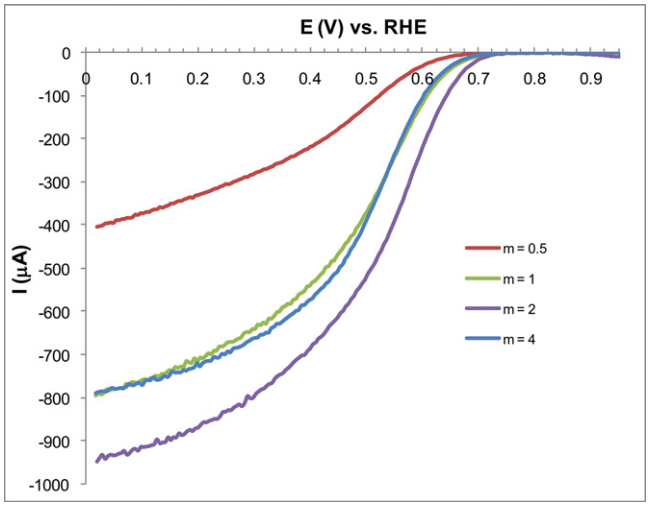

Fig. 2. Linear sweep voltammetry of catalysts with different CB:PPY weight ratios m and equal PY:Co molar ratios $p = 2$ at a rotation rate of 1500 rpm and a scan rate of 5 mV/s, in a $HClO_4$ buffer at pH = 1.

to the ORR: the higher the ORR activity, the closer $E_{P,C}$ is to the thermodynamic potential of 1.17 V [6]. The data from CV show that the catalyst with $m = 0.5$ is the least active, and although the other three catalysts have $E_{P,C}$ that are quite close, the two ratios $m = 1$ and $m = 2$ give better performances with similar activities.

To better distinguish between the performances of the four catalysts, LSV at 1500 rpm was conducted and outcomes of these experiments are provided in Fig. 2 and Table 2. The voltammogram for $m = 2$ unambiguously indicates that this material is the best among the four, with a curve shifted to higher potentials compared to the others and the largest limiting current i_L at lowest potentials. This translates into the highest onset potential for $m = 2$, with the onset potential here being defined as the potential from which the current starts to be larger than 1 μA (at which point noise contributions can be overlooked). To confirm the hierarchy in activity between the four catalysts, their currents at a disk potential of 0.65 V were compared and their mass activities were deducted (Table 2). That potential of 0.65 V was chosen since it was sufficiently remote from the onset potentials to give currents that were large enough to be accurately compared, but close enough to these onset potentials so that the currents were mostly due to the products of the kinetics of reaction, with a negligible contribution from diffusion—the latter phenomena starting in our case to contribute to the currents at potentials lower than 0.6 V. Comparison of the mass activities demonstrate that while $m = 1$ and $m = 4$ lead to comparable activities, the CB:PPY weight ratio of $m = 2$ resulted in the best activity, with a mass activity that is more than twice that for $m = 1$ and $m = 4$. It is worth mentioning that the catalyst that corresponds to $m = 4$ (and $p = 2$), i.e., Co_2PPYCB_4, has a composition that is close to the one used in reference articles concerning such catalysts [10,13].

Following the above determination, two more catalysts were prepared, with the same CB:PPY weight ratio $m = 2$, but with PY:Co molar ratios of $p = 4$ and $p = 1$. The CV curves for the three materials ($p = 1$, 2, and 4) all exhibited $E_{P,C}$ peaks that were practically at the same position, although the peak intensities, and thus catalytic activities, increased with p (Fig. 3). On the other hand, the LSV curves for the three catalysts (Fig. 4) suggest that the catalyst with $p = 1$ is the least active, since its curve is the most shifted to the lower potentials. By a similar argument, the curve for $p = 4$ appears to represent the most active catalyst. Determination of mass activities at 0.65 V (Table 2) confirms the relationship between the PY:Co molar ratio p and catalytic activity for a CB:PPY weight ratio $m = 2$.

Table 2
Kinetic data of the catalysts.

	CB:PPY (wt.)	PY:Co (mol.)	$E_{P,C}$ (V)	E_{onset} (V)	I at 0.65 V (μA)	m_{cata} (μg)	Mass activity at 0.65 V (A/g_{cata})
$Co_2PPYCB_{0.5}$	0.5	2	0.517	0.712	10	100	0.10
Co_2PPYCB_1	1	2	0.546	0.741	41	100	0.41
Co_2PPYCB_2	2	2	0.551	0.746	86	80	1.08
Co_2PPYCB_4	4	2	0.532	0.736	34	70	0.49
Co_4PPYCB_2	2	4	0.565	0.785	114	110	1.04
Co_1PPYCB_2	2	1	0.566	0.766	59	120	0.49

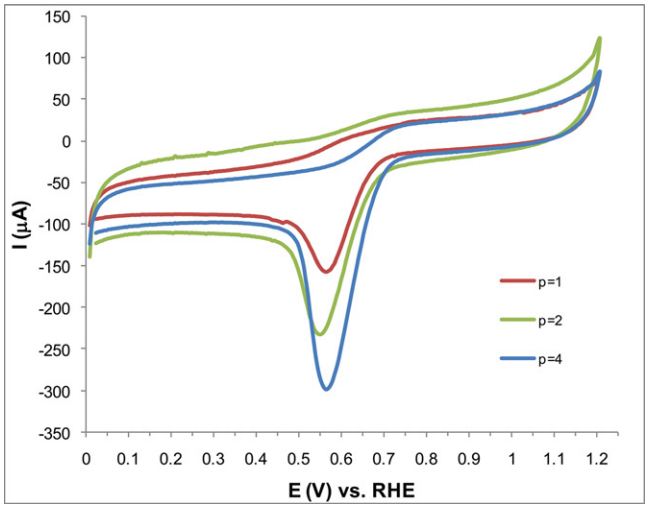

Fig. 3. Cyclic voltammetry of catalysts with different PY:Co molar ratios p and equal CB:PPY weight ratios $m = 2$ at a scan rate of 10 mV/s, in a $HClO_4$ buffer at pH = 1.

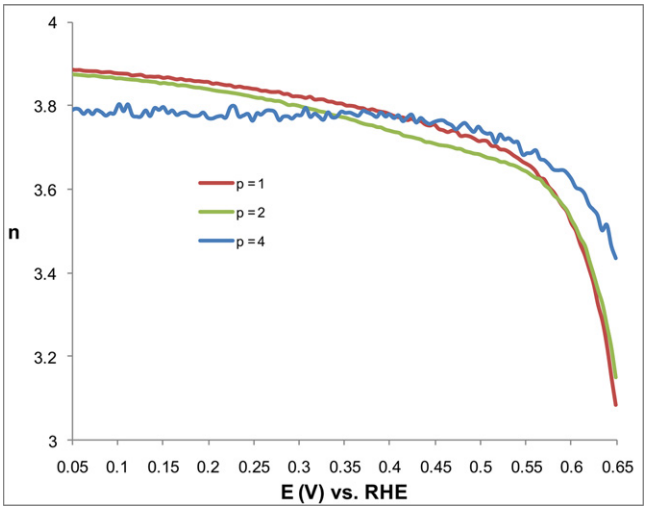

Fig. 5. Plot of n (number of e^- exchanged) as determined by RRDE vs. potential.

However, the $p = 2$ and $p = 4$ catalysts have activities that are similar. These two catalysts nevertheless markedly differ in their limiting currents i_L, which are the disk currents at low potentials ($E = 0.01$ V). At such potentials, disk currents are mostly the result of O_2 diffusion to the disk instead of the reaction kinetics there.

With equivalent mass activities, the more interesting catalyst for fuel cells between $p = 2$ and $p = 4$ would be the one whose number of e^- exchanged during the ORR, n, is closer to the theoretical value of 4 and does not instead promote the $2e^-$ process of peroxide

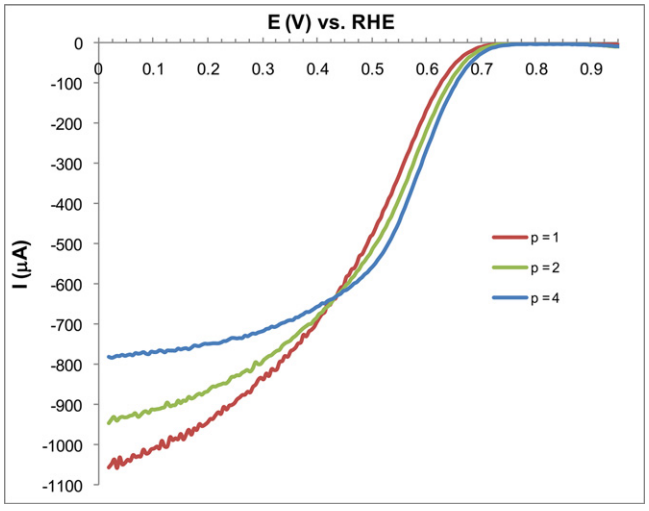

Fig. 4. Linear sweep voltammetry of catalysts with different PY:Co molar ratios p and equal CB:PPY weight ratios $m = 2$ at a rotation rate of 1500 rpm and a scan rate of 5 mV/s, in a $HClO_4$ buffer at pH = 1.

formation, as shown below:

$$O_2 + 2H^+ + 2e^- \rightarrow H_2O_2 \qquad E^0_{cathode} = 0.70\,V$$

The peroxide thus formed either is released into the bulk solution as a byproduct or undergoes further reduction to H_2O, in which case the net reaction is that O_2 is reduced to H_2O through an indirect $4e^-$ pathway, as shown below:

$$H_2O_2 + 2H^+ + 2e^- \rightarrow 2H_2O \qquad E^0_{cathode} = 1.78\,V$$

In general, peroxide formation should be avoided to the highest extent possible as it reduces the energy efficiency of fuel cells, damages the Nafion membrane, and may play a role in the deactivation of the catalyst [5]. Thus, an n value closer to 4 should result in a lower amount of peroxide being generated.

The RRDE setup allows the determination both of n and the % of H_2O_2 produced (see Eqs. (1) and (2) below) [5]:

$$n = 4\frac{I_D}{I_D + I_R/N} \tag{1}$$

$$\%H_2O_2 = 100\frac{2I_R/N}{I_D + I_R/N} \tag{2}$$

in which N is the previously defined collection efficiency, I_R is the ring current, and I_D is the disk current. These two equations were used to determine n and $\%H_2O_2$ for a CB:PPY weight ratio of $m = 2$ and a PY:Co molar ratio of $p = 1$, 2, and 4, and the results are plotted in Figs. 5 and 6. It can be seen from these figures that for potentials larger than 0.6 V, i.e., for voltages that are relevant to fuel cell operations, the catalysts with $p = 1$ and $p = 2$ have values of n and $\%H_2O_2$ that are very similar, which suggests that they both produce peroxide to the same degree. But the catalyst corresponding to $p = 4$ has an n that is closer to 4 and a $\%H_2O_2$ value that is lower than those for the other two materials, which indicates that the former catalyst reduces O_2 to H_2O through a $4e^-$ mechanism to a larger

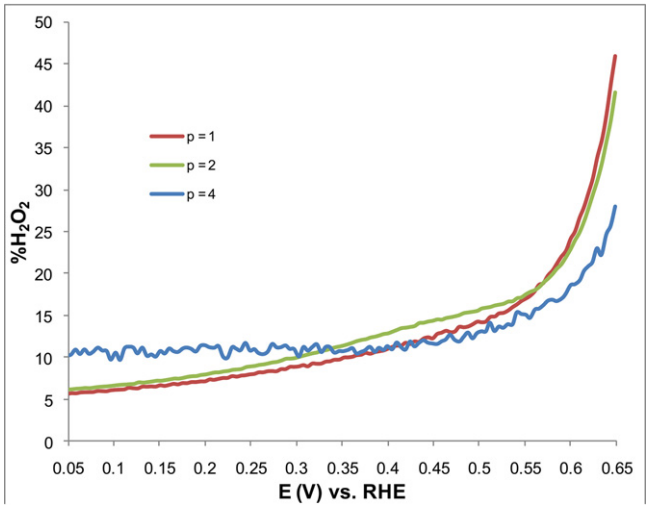

Fig. 6. Plot of $\%H_2O_2$ as determined by RRDE vs. potential.

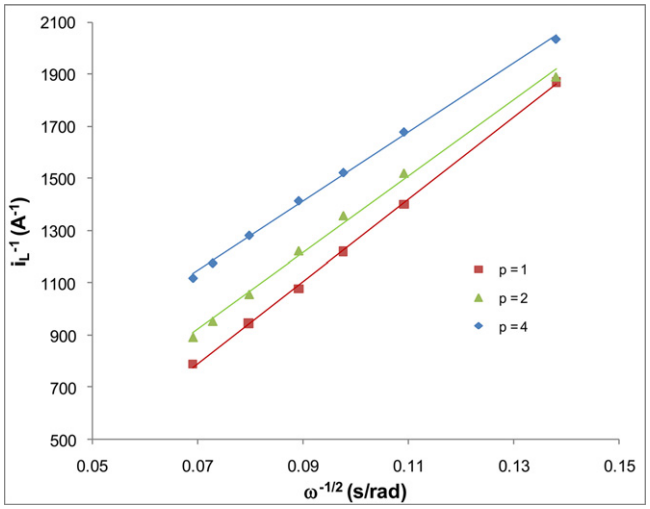

Fig. 7. Plots of the limiting current i_L vs. $\omega^{-1/2}$ for the catalysts with a CB:PPY weight ratio $m = 2$ and a PY:Co molar ratio of $p = 1$, 2, and 4.

extent than do the latter ones. Values of n and $\%H_2O_2$ for the three materials for $E = 0.65$ V are provided in Table 3, and show that, at this voltage, the $\%H_2O_2$ for $p = 1$ and $p = 2$ are about 50% higher than that for $p = 4$.

The number of e^- exchanged n can also be found through the Koutecky–Levich $1/i$ vs. $\omega^{-1/2}$ plot [13]:

$$\frac{1}{i} = \frac{1}{i_k} + \frac{1}{i_d} \tag{3}$$

$$i_d = 0.62nFC_{O_2}D_{O_2}^{2/3}\nu^{-1/6}\omega^{1/2} \tag{4}$$

with i being the total disk current, i_k is the kinetic current, i_d is the diffusion current, $F = 96485$ C mol^{-1} is the Faraday constant, C_{O_2} is the concentration of O_2 in the electrolyte, D_{O_2} is the diffusion coefficient of O_2 in the electrolyte, ν is the kinematic viscosity of the electrolyte, and ω is the rotation rate of the disk electrode.

At low potentials, the ORR is diffusion-controlled and i_d equates to i_L, the limiting current. And, a plot of i_L^{-1} vs. $\omega^{-1/2}$ should yield n. This plot was done for the catalysts with a CB:PPY weight ratio $m = 2$ and a PY:Co molar ratio of $p = 1$, 2, and 4 (Fig. 7), using the values $D_{O_2} = 1.9 \times 10^{-5}$ cm^2 s^{-1}, $C_{O_2} = 1.18 \times 10^{-6}$ mol cm^{-3}, and $\nu = 9.87 \times 10^{-3}$ cm^2 s^{-1} [17]. All three plots gave straight lines with a correlation coefficient larger than 0.99. It is noted that not only does the method give the same pattern as the RRDE setup, which is that n approaches 4 as p is increased, but the values of n determined by the two procedures nearly agree (Table 3). Overall, it appears that among the seven catalysts studied, the one with a CB:PPY weight ratio $m = 2$ and a PY:Co molar ratio $p = 4$ is the one that comes closest to our needs for fuel cell applications, having a relatively high mass activity and producing a $\%H_2O_2$ yield that is not too large. This particular catalyst, Co_4PPYCB_2, had its kinetic activity for the ORR compared to that of the state-of-the-art commercial Pt catalyst ETEK (10 wt.% Pt).

ETEK was deposited on the glassy carbon disk following a procedure similar to that used for the Co–PPY–CB catalysts; the amounts used are reported in Table 1. Fig. 8 compares the linear sweep voltammetry experiments for ETEK and Co_4PPYCB_2 under the same conditions. The E_{onset} for ETEK is clearly larger and closer to the thermodynamic potential of 1.17 V than that for Co_4PPYCB_2. An inspection of the data for ETEK reveals an E_{onset} of 0.911 V, which represents a difference of 126 mV compared with E_{onset} for Co_4PPYCB_2. Linear sweeps with ETEK carried out at different rotation rates (not shown) indicated that for potentials lower than 0.8 V diffusion phenomena significantly contribute to the disk current, which implies that kinetic currents for Co_4PPYCB_2 and ETEK cannot be directly compared, since E_{onset} for Co_4PPYCB_2 is lower than 0.8 V. Thus, as another way to compare the kinetic activities of the two catalysts, the voltages at which they rendered a mass activity of 1 A/g_{cata} were determined. It was found that the potentials had values of 0.649 V and 0.849 V, respectively, for Co_4PPYCB_2 and ETEK, which amounted to a difference of 200 mV.

The number of e^- exchanged (n) and $\%H_2O_2$ for ETEK were calculated through Eqs. (1) and (2), and the results are plotted in Figs. 9 and 10. Based on those two figures, it can be seen that at higher potentials, n is closer to 3 than 4 and $\%H_2O_2$ is relatively high, with *ca.* 5% of H_2O_2 formed for potentials lower than 0.7 V. For a fair comparison to Co_4PPYCB_2, n and $\%H_2O_2$ for ETEK were determined at a voltage of 0.85 V, at which noise contributions to

Table 3
n (number of e^- exchanged) as determined by RRDE at 0.65 V and the Koutecky–Levich plot at 0.01 V, and $\%H_2O_2$ determined by RRDE at 0.65 V.

	PY:Co (mol.)	n_{RRDE}	$\%H_2O_2$	n_{KL}
Co_1PPYCB_2	1	3.1	46	3.0
Co_2PPYCB_2	2	3.2	42	3.2
Co_4PPYCB_2	4	3.4	28	3.6

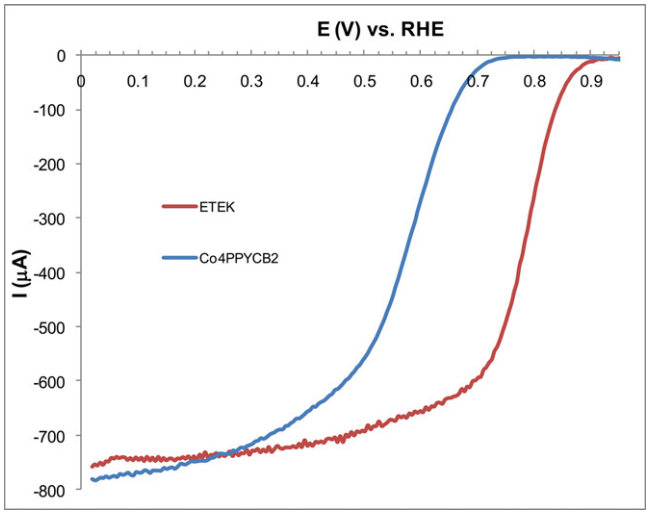

Fig. 8. Linear sweep voltammetry of Co_4PPYCB_2 and ETEK at a rotation rate of 1500 rpm and a scan rate of 5 mV/s, in a $HClO_4$ buffer at pH = 1.

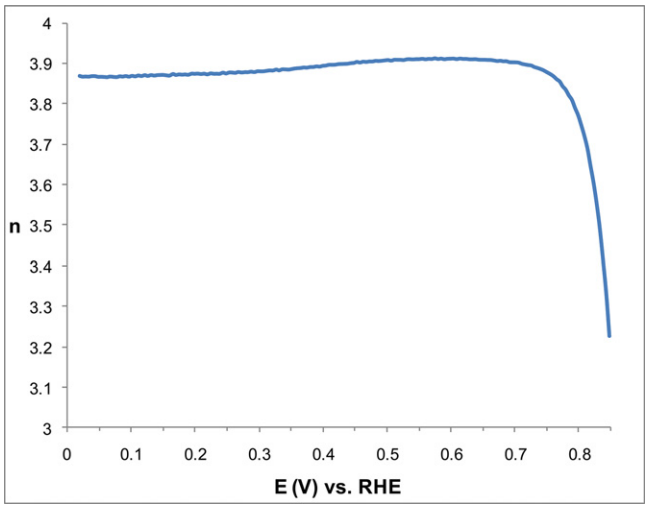

Fig. 9. Plot of n (number of e^- exchanged) vs. potential for ETEK.

the current and diffusion phenomena can be neglected. The values thus obtained for ETEK were 3.2 and 39, respectively. At 0.65 V, Co_4PPYCB_2 had $n = 3.4$ and $\%H_2O_2 = 28$, and hence compares favorably to ETEK at realistic fuel cell operating voltages.

Based on the electrochemical results, we focused our attention on catalysts with a CB:PPY weight ratio $m = 2$ and a PY:Co molar ratio $p = 1$, 2, and 4 for characterization and determination of the active sites for ORR. XRD was thus performed on these catalysts and on the carbon black (CB) support (Fig. 11). The pattern for CB contains peaks at 24.6° and at 43.5° that are attributable, respectively, to the (0 0 2) and (1 0 0) planes of graphitic C. Aside from the (0 0 2) peak of CB, the catalysts all exhibit peaks at 44.2° and 51.4°, which, respectively, are assigned to the (1 1 1) and (2 0 0) planes of metallic α-Co, the former peak overshadowing the (1 0 0) peak from CB. All three catalysts thus contain Co under crystalline form. Nevertheless, the peak intensities from Co decrease with the Co content, which hints at smaller Co particles for lower Co loadings. The average diameter d of these Co particles can be estimated using the Scherrer equation:

$$d = \frac{0.9\lambda}{\beta \cos\theta} \quad (5)$$

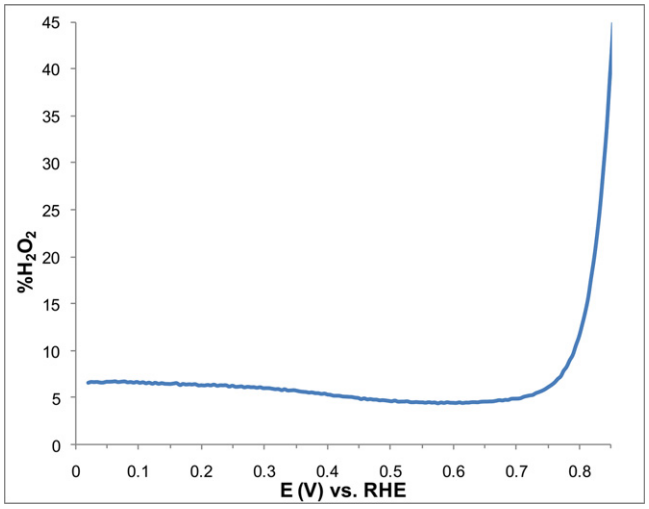

Fig. 10. Plot of $\%H_2O_2$ vs. potential for ETEK.

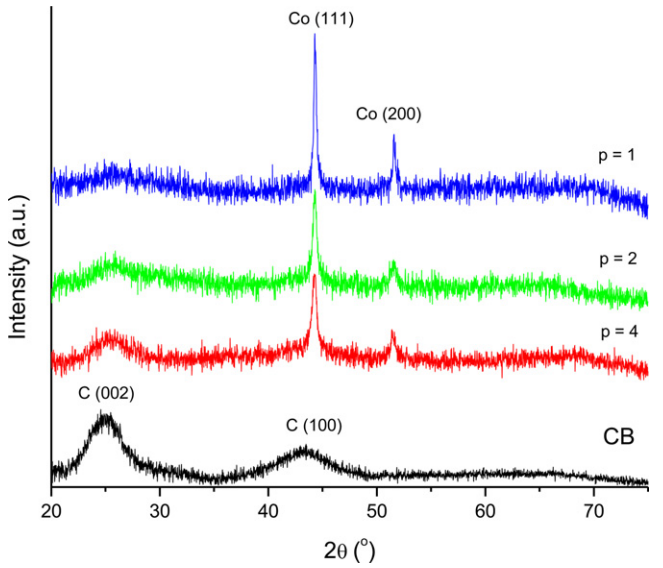

Fig. 11. XRD patterns of carbon black (CB) and of the catalysts with a CB:PPY weight ratio of $m = 2$ and a PY:Co molar ratio of $p = 1$, 2, and 4.

in which λ is the wavelength of the X-ray radiation (1.54056 Å), β is the full width at half maximum (FWHM) of the peak (in radians), and θ is the diffraction angle. To calculate d, the (1 1 1) peaks were used and fitted to Lorentzians. It was found that the catalysts for $p = 1$, 2, and 4 contained Co nanoparticles that were, respectively, on average, 29.9, 18.3, and 15.8 nm wide.

Additionally, TEM images have been acquired to get more precise structural information for our catalysts. The micrograph for CB (Fig. 12A) shows a material consisting of particles that are between 10 and 100 nm wide that aggregate and form layers. The CB/PPY composite support with a CB:PPY weight ratio $m = 2$, which was used to prepare the three catalysts, was also analyzed by TEM (Fig. 12B). The micrograph reveals that the support only has one type of particle, indicating that PPY did not form a separate phase from CB, but instead was deposited entirely on the surface of the CB particles. However, the particles in the composite are clearly larger than those for CB alone. Close examination of Fig. 12B suggests that PPY forms a thin film on the surface of CB particles and agglomerates the latter ones into larger clusters.

We also note that the three Co-containing catalysts clearly show Co nanoparticles (Fig. 12C–H), although differences can be found in the size and in the degree of dispersion of the nanoparticles on the surface of these catalysts. The nanoparticle sizes were determined by the ImageJ software. The catalyst corresponding to $p = 1$, i.e., the one with the highest Co content, consists mostly of large Co nanoparticles, with diameters in the range of 30–35 nm, although particles smaller than 10 nm are also present. Also, Co nanoparticles are not uniformly dispersed, as Co nanoparticles-free areas coexist along with Co nanoparticles-rich areas. For $p = 2$, Co nanoparticles are found to be much more dispersed on the catalyst, with most having a width between 15 and 25 nm, although particles as large as 70 nm can be found. In the case of $p = 4$, Co nanoparticles are only present in certain areas of the catalyst, as is the case with $p = 1$. However, with $p = 4$, the particles are smaller, with diameters generally in the 15–20 nm range, although a few particles with a size of around 55 nm also exist. In general, XRD and TEM analyses agree: as the Co content decreases, so does the average size of the Co nanoparticles. Furthermore, we note that the average sizes of the majority of the particles determined by TEM closely match the average sizes found through the Scherrer equation with XRD.

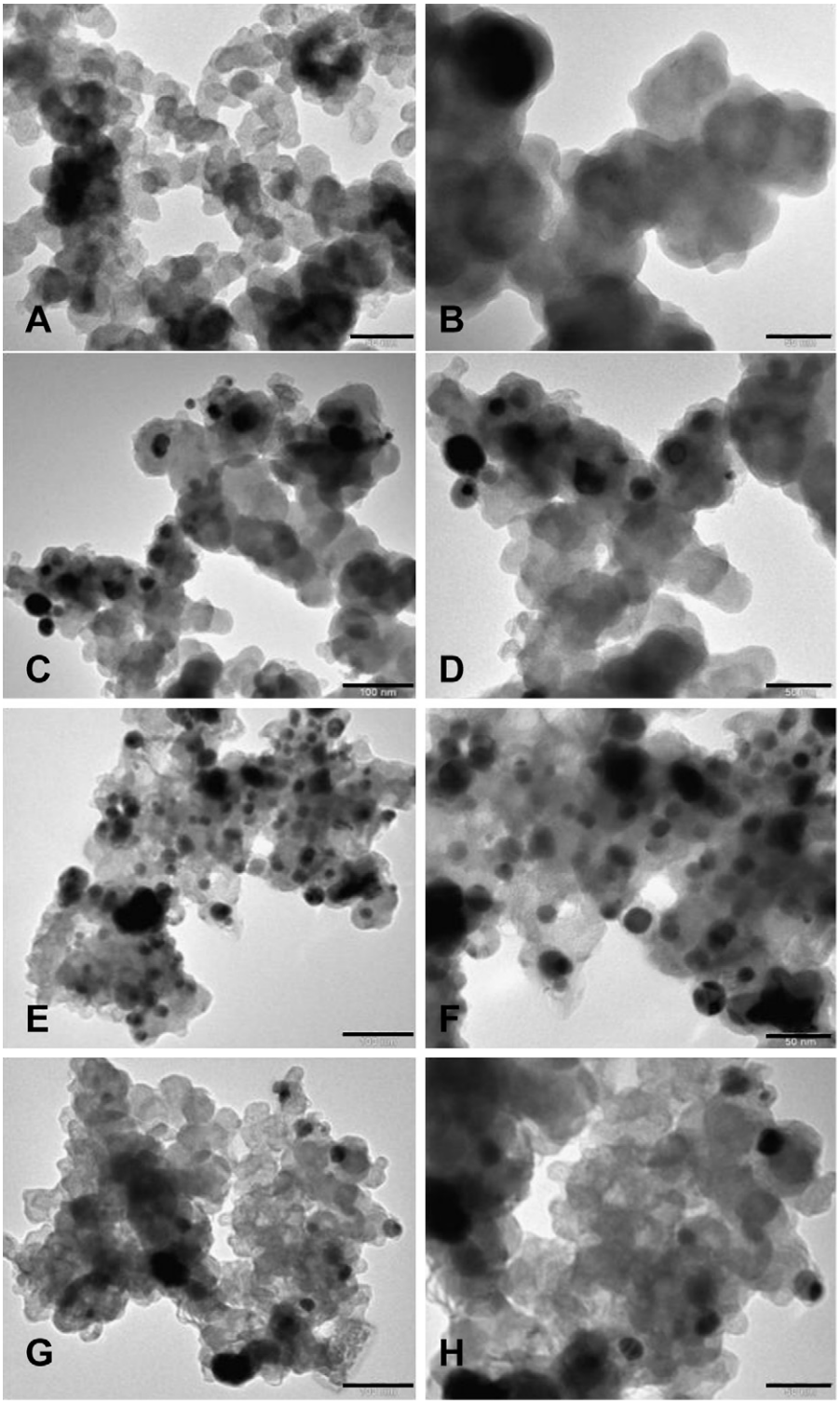

Fig. 12. TEM micrographs of (A) CB, (B) CB–PPY composite support for a CB:PPY weight ratio of $m = 2$, (C) Co_1PPYCB_2 ($m = 2$, PY:Co molar ratio of $p = 1$), (D) Co_1PPYCB_2 ($m = 2$, $p = 1$), (E) Co_2PPYCB_2 ($m = 2$, $p = 2$), (F) Co_2PPYCB_2 ($m = 2$, $p = 2$), (G) Co_4PPYCB_2 ($m = 2$, $p = 4$), (H) Co_4PPYCB_2 ($m = 2$, $p = 4$); scale bars = 100 nm for (C), (E), and (G) (140k× magnification) = 50 nm for (A), (B), (D), (F), and (H) (250k× magnification).

EDS mapping of the best performing catalyst Co_4PPYCB_2 ($m = 2$ and $p = 4$), using the Kα line of N and the Lα line of Co, shows that, while N is present throughout the sample (Fig. 13B), Co nanoparticles (NPs) in fact coexist with isolated Co atoms (or small clusters) that are well-dispersed on that material (Fig. 13C).

EDS was also used to determine the N:Co atomic ratios in the catalysts prior to and following calcination. The particles analyzed for each catalyst gave various ratios, some of them being lower than 1, which indicates formation of Co nanoparticles or clusters even without calcination as Co^{2+} was reduced to Co by $NaBH_4$ in solution. It should be noted that the proportion of ratios lower than 1 increased with Co content, regardless of whether the considered material had been calcined or not. Overall, the samples all showed some degree of heterogeneity. However, for each one, certain N:Co

Table 4
N:Co atomic ratios of the catalysts prior to and following calcination with CB:PPY weight ratios $m = 2$ and PY:Co molar ratios $p = 1$, 2, and 4.

	Co_1PPYCB_2 (uncalcined) $p = 1$	Co_2PPYCB_2 (uncalcined) $p = 2$	Co_4PPYCB_2 (uncalcined) $p = 4$	Co_1PPYCB_2 (calcined) $p = 1$	Co_2PPYCB_2 (calcined) $p = 2$	Co_4PPYCB_2 (calcined) $p = 4$
N:Co	2.06 (±0.10) 1.36 (±0.21)	2.70 (±0.17) 2.01 (±0.05) 1.65 (±0.06)	3.42 (±0.06) 3.00 (±0.02) 1.45 (±0.01)	1.26 (±0.10)	2.75 (±0.05) 2.25 (±0.12) 1.73 (±0.12) 1.33 (±0.01)	2.95 (±0.02) 2.29 (±0.03) 1.72 (±0.15)

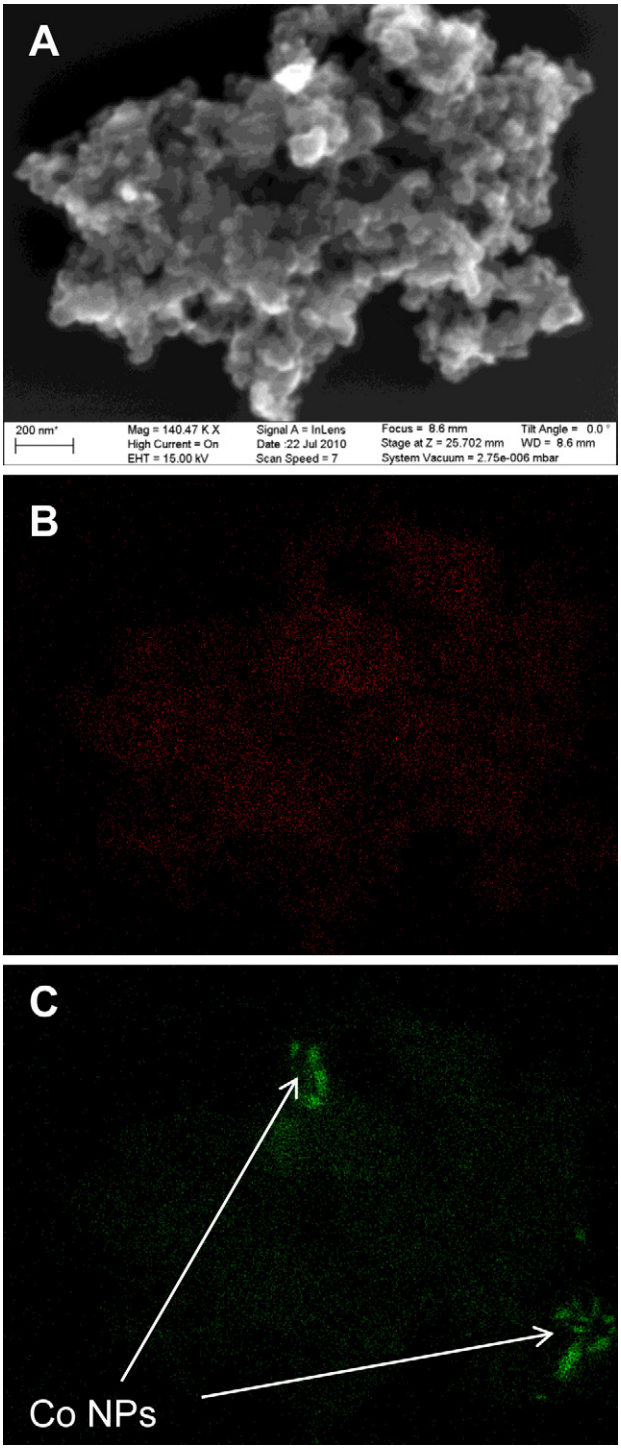

Fig. 13. (A) SEM micrograph of Co_4PPYCB_2 ($m = 2$ and $p = 4$), (B) N and (C) Co EDS mapping (15 kV) of the same particle, scale bar = 200 nm (140k× magnification).

atomic ratios were consistent with one another, and those ratios are reported in Table 4. Before calcination, for PY:Co molar ratios $p = 1$ and $p = 2$, it was found that out of a dozen particles studied, at least one third of them had a N:Co ratio under 1 while for $p = 4$, this was the case for only two particles, so $p = 1$ and $p = 2$ lead to the formation of more Co nanoparticles than $p = 4$. It can also be deducted that the N:Co ratios determined increase with p. After calcination, the N:Co ratios for all three catalysts are lower than those for their respective precursors, which must be a result of both loss of N and Co aggregation. Furthermore, more than half of the particles analyzed for $p = 1$ gave N:Co ratios lower than 1, whereas for $p = 2$ and $p = 4$, those ratios were less than 1 for only a couple of particles, so the latter catalysts have formed nanoparticles to a much lower degree than the former one. In general, the catalysts with $p = 2$ and $p = 4$ have similar N:Co ratios, although the one with $p = 4$ did not render ratios around 1.3 as the other two catalysts did.

For a better understanding of the local structure of the Co atoms in the catalysts, we utilized EXAFS analysis. The Co K-edge EXAFS spectra in r space of the catalysts (after calcination) all show the same features as those found for bulk Co, with peaks at 2.1, 3.9, and 4.7 Å (Fig. 14A). However, Co K-edge EXAFS data of the same samples prior to heat treatment reveal unique, non-bulk features (Fig. 14B). Data analysis shows significant differences in coordination numbers and bond distances between the pre-treated samples. First-shell coordination numbers (N) and bond distances (r) of Co–Co and Co–N/O determined by curve-fitting are reported in Table 5 (note: N/O represents nitrogen/oxygen, with the two atoms not distinguishable by this technique, with the latter coordination likely due to the presence of acetate ions from the Co salt) while the corresponding simulated functions can be found in Fig. S1 in the Supplementary Data. Based on the latter data, it can be seen that the precursors with $p = 2$ and $p = 4$ have Co atoms with similar local coordination environments, with most notably about 6 N/O atoms attached. It should be pointed out that these two precursors are the ones for the two best catalysts, with equivalent ORR activities. On the other hand, the uncalcined catalyst with $p = 1$ has its Co atoms surrounded by 3 N/O atoms, and the resulting catalyst had lower ORR activity.

4. Discussion

The catalysts synthesized in this study were prepared with a method that is easy to follow and allows the incorporation on the CB surface of N without requiring a pretreatment of CB with concentrated strong acids. Indeed, based on TEM analysis, PPY seems to have a strong affinity for CB and easily deposits onto the surface of the latter. That affinity likely stems from the attraction between the aromatic rings that constitute PPY and the graphitic character

Table 5
Coordination numbers (N) and distances (r) of Co to Co and O/N atoms as determined by curve-fitting of the Co K-edge EXAFS spectra.

	N_{Co}	$r_{Co–Co}$ (Å)	$N_{N/O}$	$r_{Co–N/O}$ (Å)
Co_1PPYCB_2 ($p = 1$)	4.2 (±2.4)	2.90 (±0.03)	2.9 (±1.0)	1.94 (±0.02)
Co_2PPYCB_2 ($p = 2$)	0.7 (±0.3)	3.11 (±0.02)	6.0 (±2.1)	2.02 (±0.03)
Co_4PPYCB_2 ($p = 4$)	3.8 (±1.3)	3.14 (±0.02)	5.5 (±1.2)	2.06 (±0.02)

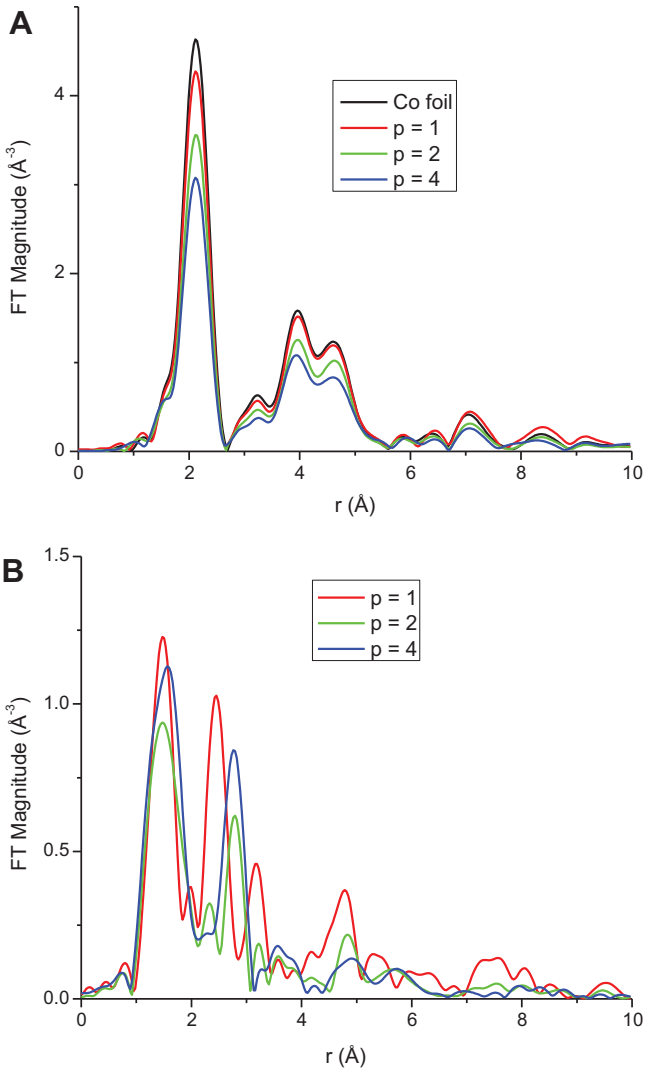

Fig. 14. Fourier-transformed Co K-edge k^2-weighted EXAFS spectra of the catalysts (m = 2 and p = 1, 2, and 4) after (A) and before (B) calcination.

of CB. Such a facile interaction between PPY and CB permits control of the amounts of N that can be deposited onto CB, which would not be the case if, for example, NH_3 were employed as the N source [5,6,14], allowing those N amounts to be finely tuned to render the best possible efficiency for ORR with such catalysts.

The first step of our work consisted in determining the best CB:PPY weight ratio m. It was found that the ORR activity increased as m changed from 4 to 2, then decreased as m decreased from 2 to 0.5. This can be understood if PPY is considered as merely being an N source. Indeed, it is expected that following calcination at 900 °C under Ar, PPY is totally converted into C and N atoms, of which some are lost, with the remaining N incorporated into the CB matrix and/or coordinated to Co. As such, the ORR activity would increase from m = 4 to m = 2 as more N atoms are deposited, and thus more ORR active sites created on the C surface. For m values lower than 2, corresponding to higher N contents, the kinetics of ORR are lower: this is likely the result of the oversaturation of the CB surface with the products of decomposition from PPY. Such oversaturation could lead to a loss of porosity from the CB through the filling of the smaller pores, which would be detrimental to the ORR activity. Indeed, it has been shown that porosity is a significant factor for ORR with this type of catalysts, as the more active sites are located in micropores [14] or mesopores [18]. It is also possible that for larger fractions of PPY ($m \leq 1$), the polymer would generate layers on the CB surface that are so thick that the additional N atoms are too far from the CB surface to efficiently contribute to the ORR.

Following the determination of the optimum CB:PPY weight ratio, PY:Co molar ratios p equal to 1, 2, and 4 were used with the optimum CB:PPY weight ratio to formulate catalysts. Comparison between the mass activities revealed that ratios of 2 and 4 gave better results. It is to be noted that such ratios were chosen as studies on similar materials, that contained Fe instead of Co, revealed the existence of FeN_2 and FeN_4 sites by time of flight secondary ion mass spectroscopy, with preponderance of the former sites in the catalytic process of ORR [5,19]. Additionally, it has been found that although the two molar ratios of 2 and 4 gave similar mass activities, the selectivities to H_2O formation that they lead to differ, with the catalyst having a PY:Co molar ratio p = 4 producing less H_2O_2, and thus having a number of e^- exchanged (n) closer to 4. However, considering the relatively high percentage of H_2O_2 produced by the catalyst with p = 4, it is likely that, in fact, O_2 undergoes an indirect $4e^-$ reduction to H_2O on that catalyst, with reduction of the H_2O_2 intermediate [7]. Nevertheless, the PY:Co molar ratio p in the precursor is important for both the kinetic activity and the selectivity of such catalysts.

XRD and TEM results indicate that for all three p molar ratio values, crystalline nanoparticles of Co were present. However, Co on CB only has a negligible activity for ORR [10], so the kinetic activities observed with these catalysts should not originate from these nanoparticles. On the other hand, although in catalysts such as ours ORR activity is usually associated with the presence of MeN_x sites, some groups attribute it to the presence of various kinds of N atoms (incorporated with the help of the metal) within the carbon matrix during the calcination process [9,15]. Nevertheless, it has been demonstrated that materials similar to ours do possess significant ORR activity even without calcination, and that the latter procedure only moderately improves this already existing activity [11,13]. Hence, the catalytic activity of our materials should originate from CoN_x sites, not just N atoms.

TEM analysis unambiguously shows that the most active and most selective catalyst, with p = 4, contains the smallest Co nanoparticles and has the least area covered with these particles. As p decreases to 2, more catalyst area is covered with Co nanoparticles that are a bit larger. For p = 1, however, Co NPs occupy less area and they are much larger on average than the ones observed for p = 2 and p = 4. The increase in Co nanoparticles surface coverage as p decreases from 4 to 2 can be interpreted as a general increase in Co density as the Co content increases. The decrease in Co nanoparticles coverage and the significant increase in particle size as p decreases from 2 to 1 possibly stems from the sintering of the nanoparticles as the Co density is increased. It is thus reasonable to assume that, as p decreases (i.e., as the amount of Co increases), but with the C:N atomic ratio remaining the same, fewer Co atoms form CoN_x sites and those that do not are instead driven to coalesce and generate nanoparticles. Those nanoparticles not only have poor activity for the ORR, but also may render inaccessible active CoN_x sites by superimposing the latter ones. This would explain the differences in activity as p varies. However, TEM cannot detect the presence of potential CoN_x sites.

While EDS mapping did confirm the formation of Co nanoparticles, that technique also clearly demonstrated the coexistence on the best performing catalyst, Co_4PPYCB_2, of isolated Co and N atoms throughout the entire material. As such, those atoms most probably should lie in sufficiently close proximity to give rise to CoN_x sites that can catalyze the ORR. Indeed, though some groups believe that heat treatment at 800 °C or higher temperatures entirely decomposes the Co–N complexes in the precursors and eliminates the metal–N bonds in such materials [20], XPS data have indicated the possibility of the persistence of Co–N bonds in materials similar to ours even at temperatures as high as 800 °C [13]. Furthermore,

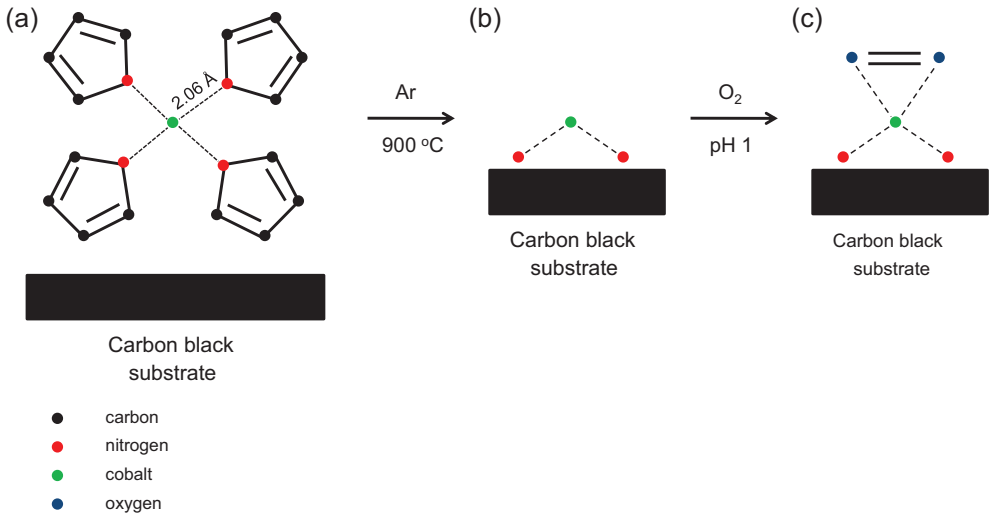

Fig. 15. Schematic representation of (A) Co_4PPYCB_2 before calcination, (B) Co_4PPYCB_2 after calcination, and (C) the presumed intermediate formed between calcined Co_4PPYCB_2 and O_2 in acidic medium.

EXAFS studies have pointed out the stability and resistance of the Co–PPY structure upon heat treatment, with shortening of the Co–Co and Co–N distances [11].

Detailed EDS analysis on several particles for each catalyst gave a better idea about the actual distribution of N and Co in the catalysts, before and after calcination. It was thus found that prior to heat treatment, the $p=1$ and $p=2$ ratios yielded much more Co nanoparticles than the $p=4$ one. This seems to indicate that in the former cases, the Co content is so high that there are not enough N atoms to form complexes with all the Co atoms, and that the excess Co instead leads to nanoparticle formation. Also, in those precursors, the determined N:Co ratios increase with p, which would hint that Co atoms forming complexes coordinate to more N atoms as p increases. Likely as p increases the Co atoms are more tightly bound to the N atoms through charge transfer from N to Co [10], as the coordination of the former ones increases. The Co–N interaction would be particularly strong for $p=4$ and would prevent nanoparticle formation. It should be noted that the N:Co ratios approach 4 in the precursor with $p=4$, which results in the best performing catalyst, and that this ratio corresponds to the assumed coordination of Co to N in such catalysts [11,21].

EDS of the calcined catalysts showed that for the least active one, with $p=1$, a significantly large fraction of the Co existed in the form of nanoparticles, which is not the case for the other two catalysts. Moreover, the N:Co ratios for the former were the lowest. Interestingly, we find that for $p=2$ and $p=4$, the N:Co ratios are very similar while the corresponding mass activities for ORR are equivalent. The major differences between the catalyst with $p=2$ and that with $p=4$ is the better selectivity of the latter and the absence of N:Co ratios around 1.3, as was found for the catalysts with $p=1$ and $p=2$, which might suggest that lower N:Co ratios close to 1 tend to produce H_2O_2 to a greater extent. Overall, EDS analysis of calcined catalysts indicates that better ORR activity and selectivity are obtained when sites with N:Co ratios of around 2 are present, which would support the findings of Lefevre et al. [5,19].

Co K-edge EXAFS analysis of the calcined catalysts verified the presence of large (several nm in size) Co particles. For this size of particles, EXAFS is not sensitive to the non-bulk effects and to the presence of any metal–nonmetal bonding, due to the bulk metal Co–Co contributions dominating the data. However, EXAFS carried out on the precursors was much more informative. It confirmed the results from EDS that in the precursor for the least active catalyst, with $p=1$, Co has a low coordination number with N/O. On the other hand, EXAFS underlined the close similarity, i.e., equivalent coordination numbers to N/O and bond distances to N/O, of the Co complexes in the precursors with $p=2$ and $p=4$, with those materials giving the two better and nearly equally performing catalysts. For both precursors, it was found that Co is surrounded by 6 atoms of N and/or O. From EDS, out of those 6 neighbors, 2 or 3 of them would be N atoms for $p=2$, while 3 or 4 of them would be N atoms for $p=4$.

Based on the results from EDS and EXAFS, it appears that for the best performing catalyst Co_4PPYCB_2 ($p=4$), that is also the one that generates the least peroxide, Co coordinates to nearly 4 N in the precursor, those complexes yielding highly ORR active CoN_2 sites upon calcination. The coordination of Co in the latter sites could favor the adsorption on them of O_2 through charge transfer from free electron pairs on O to Co, similarly to what happens between N and Co. This would result in the formation of an intermediate in which Co is again coordinated to 4 ligands (Fig. 15). The strong electronic interactions existing in that intermediate could weaken the O=O bond and facilitate its breaking, which would thus favor ORR and limit peroxide formation. In the case of CoN_1 sites, O_2 would adsorb less strongly as the resulting intermediate would have 3 ligands around Co instead of 4, which would explain the lower activities and/or selectivities found for Co_1PPYCB_2 ($p=1$) and Co_2PPCB_2 ($p=2$).

When comparing the performance of our best catalyst, Co_4PPYCB_2, to that of ETEK, the former catalyst gave promising results, with less H_2O_2 generated at realistic fuel cell potentials (0.65 V for Co_4PPYCB_2 and 0.85 V for ETEK) and an overpotential that is 200 mV higher than that for ETEK for the same mass activity of 1 A/g_{cata}. Although the use of Co instead of Pt results in a non-negligible potential loss, considering that Co is about 600 times less expensive than Pt, Co_4PPYCB_2 appears to be a promising fuel cell catalyst, with overall quite satisfactory performances for the ORR.

5. Conclusions

By varying the CB:PPY weight ratio and the PY:Co molar ratio, it was demonstrated that the composition of Co–PPY–CB catalysts has a major influence on their ORR activity and selectivity. As such, a CB:PPY weight ratio $m=2$ allowed the deposition and/or incorporation of the highest amount of N on the CB support without oversaturation of the smaller pores needed for the

ORR. On the other hand, it was shown that a PY:Co molar ratio $p = 4$, instead of 1 or 2, leads to better ORR activity and selectivity. Based on EDS and EXAFS analysis, it is believed that a PY:Co molar ratio $p = 4$ favors the formation in the catalyst precursor of complexes in which Co is coordinated to 3 or 4 N atoms. Such coordination of Co to N would be at the origin of strong interactions between the concerned atoms, which would limit the formation of low ORR activity Co nanoparticles upon calcination of the precursor. With heat treatment, those Co–N complexes generate CoN_{x-2} sites. The particularly high ORR activity and selectivity of these sites might owe to the coordination of Co that would result in the strong adsorption of O_2 on them, which would promote ORR and restrict peroxide generation. Compared to a commercial state-of-the-art Pt catalyst, the ORR activity of the best Co–PPY–CB catalyst studied, with $m = 2$ and $p = 4$, is more than adequate, with a voltage that is about 200 mV lower but with less H_2O_2 being formed. Conceivably, an even better Co–PPY-based catalyst could be designed through the use of a carbon support that has, for example, higher porosity or better conductivity.

Acknowledgements

DLA would like to thank the National Science Foundation for support of this work under Grant No. HRD-0833180. AIF acknowledges support by DOE BES Grant DE-FG02-03ER15476. DNT would like to thank Prof. Glen R. Kowach from The City College of New York for his advice regarding various aspects of this work and for fruitful discussions. The help and professionalism of Dr. Jorge Morales from The City College of New York with SEM–EDS and TEM is also greatly appreciated. Also, use of the NSLS beamline X19A was supported by the U.S. Department of Energy, Office of Science, Office of Basic Energy Sciences, under Contract No. DE-AC02-98CH10886, supported in part by the Synchrotron Catalysis Consortium, U.S. Department of Energy Grant No DE-FG02-05ER15688.

Appendix A. Supplementary data

Supplementary data associated with this article can be found, in the online version, at doi:10.1016/j.apcatb.2011.03.034.

References

[1] R.K. Ahluwalia, X. Wang, R. Kumar, Argonne National Laboratory/U.S. Department of Energy, DOE Hydrogen Program Review: Fuel Cell Systems Analysis, May 2007.
[2] R. Jasinski, Nature 201 (1964) 1212–1213.
[3] V.S. Bagotzky, M.R. Tarasevich, K.A. Radyushkina, O.A. Levina, S.I. Andruseva, J. Power Sources 2 (1977) 233–240.
[4] J.A.R. van Veen, C. Visser, Electrochim. Acta 24 (1979) 921–928.
[5] M. Lefevre, J.-P. Dodelet, Electrochim. Acta 48 (2003) 2749–2760.
[6] D. Villers, X. Jacques-Bedard, J.-P. Dodelet, J. Electrochem. Soc. 151 (2004) A1507–A1515.
[7] L. Zhang, K. Lee, C.W.B. Bezerra, J. Zhang, J. Zhang, Electrochim. Acta 54 (2009) 6631–6636.
[8] H.-J. Zhang, Q.-Z. Jiang, L. Sun, X. Yuan, Z.-F. Ma, Electrochim. Acta 55 (2010) 1107–1112.
[9] V. Nallathambi, J.-W. Lee, S.P. Kumaraguru, G. Wu, B.N. Popov, J. Power Sources 183 (2008) 34–42.
[10] R. Bashyam, P. Zelenay, Nature 443 (2006) 63–66.
[11] M. Yuasa, A. Yamaguchi, H. Itsuki, K. Tanaka, M. Yamamoto, K. Oyaizu, Chem. Mater. 17 (2005) 4278–4281.
[12] A.L.M. Reddy, N. Rajalakshmi, S. Ramaprabhu, Carbon 46 (2008) 2–11.
[13] K. Lee, L. Zhang, H. Lui, R. Hui, Z. Shi, J. Zhang, Electrochim. Acta 54 (2009) 4704–4711.
[14] F. Jaouen, M. Lefevre, J.-P. Dodelet, M. Cai, J. Phys. Chem. B 110 (2006) 5553–5558.
[15] H. Niwa, K. Horiba, Y. Harada, M. Oshima, T. Ikeda, K. Terakura, J. Ozaki, S. Miyata, J. Power Sources 187 (2009) 93–97.
[16] M. Newville, J. Synchrotron. Rad. 8 (2001) 322–324.
[17] J. Maruyama, N. Fukui, M. Kawaguchi, I. Abe, J. Power Sources 194 (2009) 655–661.
[18] I. Herrmann, U.I. Kramm, S. Fiechter, P. Bogdanoff, Electrochim. Acta 54 (2009) 4275–4287.
[19] M. Lefevre, J.P. Dodelet, P. Bertrand, J. Phys. Chem. B 106 (2002) 8705–8713.
[20] N.P. Subramanian, X. Li, V. Nallathambi, S.P. Kumaraguru, H. Colon-Mercado, G. Wu, J.-W. Lee, B.N. Popov, J. Power Sources 188 (2009) 38–44.
[21] H.-J. Zhang, X. Yuan, W. Wen, D.-Y. Zhang, L. Sun, Q.-Z. Jiang, Z.-F. Ma, Electrochem. Commun. 11 (2009) 206–208.